IEEE Photonics Journal
An IEEE Photonics Society Publication

Invited Paper

Quantum Dots for Future Nanophotonic Devices: Lateral Ordering, Position, and Number Control

Volume 2, Number 1, February 2010

R. Nötzel

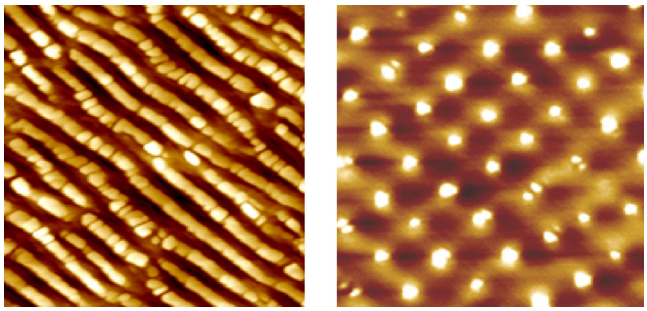

DOI: 10.1109/JPHOT.2010.2042802
1943-0655/$26.00 ©2010 IEEE

IEEE photonics SOCIETY formerly LEOS

IEEE

Quantum Dots for Future Nanophotonic Devices: Lateral Ordering, Position, and Number Control

Richard Nötzel

(Invited Paper)

COBRA Research Institute on Communication Technology, Department of Applied Physics, Eindhoven University of Technology, 5600 Eindhoven, The Netherlands

DOI: 10.1109/JPHOT.2010.2042802

Manuscript received December 16, 2009. First published Online February 8, 2010. Current version published February 23, 2010. This work was supported in part by the NanoNed program of the Stichting Technische Wetenschapen and by the Smart Mix Program of The Netherlands Ministry of Economic Affairs and The Netherlands Ministry of Education, Culture, and Science. Corresponding author: R. Nötzel (e-mail: r.noetzel@tue.nl).

Abstract: After the general aspects of InAs/InP (100) quantum dots (QDs) regarding the formation of QDs versus quantum dashes, wavelength tuning from telecom to mid-infrared region, and device applications, we discuss our recent progress on the lateral ordering, position, and number control of QDs. Single-layer and stacked linear InAs QD arrays are formed by self-organized anisotropic strain engineering of an InAs/InGaAsP superlattice template on InP (100) with emission wavelength at room temperature in the important 1.55-μm telecom wavelength region. Guided and directed self-organized anisotropic strain engineering is demonstrated on shallow- and deep-patterned GaAs (311)B for the formation of complex InGaAs QD arrays and absolute QD position control. The lateral position, distribution, and number control of InAs QDs, down to a single QD, are demonstrated on truncated InP (100) pyramids by selective-area growth with sharp emission at 1.55 μm. Submicrometer-scale active–passive integration is established by the lateral regrowth of InP around the pyramids for planarization. Such control over QD formation is the key to future quantum functional nanophotonic devices and integrated circuits operating at the single- and multiple-electron and photon level with controlled interactions.

Index Terms: Quantum dots (QDs), lateral ordering, position control, number control.

1. Introduction

Lateral ordering, position, and number control of self-organized epitaxial semiconductor quantum dots (QDs) with well-defined size and shape is the key to future quantum functional nanophotonic devices and integrated circuits [1], [2]. This will bring photonic devices and integrated circuits to the fundamental (quantum) limits regarding size, complexity, power consumption, speed, and optical nonlinearities, ultimately operating at the single- and multiple-electron and photon level with controlled quantum mechanical and electromagnetic interactions [3]–[5]. The main challenge, although it almost sounds trivial, is to develop methods for QD ordering that maintain high structural and optical quality. After general remarks on InAs/InP (100) QDs regarding formation of QDs versus quantum dashes (Qdashes) [6], wavelength tuning from telecom [7], [8] to mid-infrared region [9], and device applications [10]–[18], we discuss our recent advances toward this goal based on

self-organized anisotropic strain engineering, combination with the growth on patterned substrates, and selective-area growth with QDs operating at telecom wavelengths.

Single-layer and stacked linear InAs QD arrays are formed by self-organized anisotropic strain engineering of InAs/InGaAsP superlattice (SL) templates on InP (100) by chemical beam epitaxy (CBE) [19], [20]. The concept of self-organized anisotropic strain engineering for QD ordering has been previously introduced by us in the InAs/GaAs materials system [21]–[24] and is now transferred to the InAs/InP materials system to extend the QD emission wavelength into the important 1.55-μm telecom wavelength region. SL-template formation comprises InAs QD growth, thin InGaAsP capping, annealing, InGaAsP separation layer growth, and stacking, which leads to 1-D lateral InAs structures, i.e., lateral strain field modulations on the SL template surface governing InAs QD ordering on top due to local strain recognition. The emission wavelength at room temperature is tuned into the 1.55-μm wavelength region through insertion of ultrathin GaAs interlayers underneath the QD arrays. The QD size and wavelength increase upon strain-correlated stacking is compensated by increasing the GaAs interlayer thickness in successive layers. This demonstrates a three-dimensionally self-ordered QD crystal with fully controlled structural and optical properties.

Guided and directed self-organized anisotropic strain engineering of InGaAs/GaAs SL templates is demonstrated on coarse patterned GaAs (311)B by molecular beam epitaxy (MBE) [25], [26]. Steps generated on shallow-patterned substrates guide the self-organization process during SL template evolution for formation of complex InGaAs QD arrays. On deep-patterned substrates directed self-organization spatially locks the QD arrays to the faceted mesa sidewalls without changing the natural 2-D ordering, thus providing absolute QD position control over large areas. The absence of one-to-one pattern definition guarantees excellent optical quality of the position-controlled QD arrays which is revealed by strong photoluminescence (PL) emission at room temperature and ultrasharp PL lines from individual QDs at low temperature.

Lateral position, distribution, and number control of InAs QDs are demonstrated on truncated InP (100) pyramids by selective-area metal organic vapor phase epitaxy (MOVPE) [27]. The QD distribution and number are governed by the shape of the pyramid base and the area of the pyramid top surface, determining its facet composition. Close to pinch-off, positioning of four, three, two, and a single QD is achieved on elliptical, triangular, hexagonal, and circular-based pyramids. The single QDs reveal ultrasharp PL emission at low temperature at 1.55 μm. Lateral regrowth of InP around the pyramids establishes submicrometer active–passive integration for efficient nanophotonic devices, such as nanolasers and single-photon sources and their implementation in photonic integrated circuits.

2. General Aspects of InAs/InP (100) QDs

2.1. QDs Versus Qdashes

There is a long-lasting controversy about the formation of either InAs QDs or Qdashes and quantum wires on InP (100) [28]–[33], in particular on ternary or quaternary InGaAsP buffer layers. We unambiguously identify that the key parameter is the surface morphology of the InGaAsP buffer layer [6]. Growth conditions leading to the formation of Qdashes are always accompanied by rough buffer-layer morphology. Although other growth parameters such as higher growth temperature, larger As flux, and compressive buffer layer strain favor the formation of QDs, once the buffer layer has a rough morphology, Qdashes are formed during InAs growth. On smooth buffer layers, we always find well-shaped and symmetric QDs, independent of the substrate miscut [9]. Fig. 1(a) and (b) show the atomic force microscopy (AFM) images of the InAs Qdashes and QDs formed on the rough and smooth InGaAsP buffer layers for identical InAs growth conditions. Hence, neither the growth conditions during InAs deposition nor the substrate miscut, but rather the surface morphology of the buffer layer, determines the formation of either QDs or Qdashes, which both exhibit high optical quality.

2.2. QD Wavelength Tuning Into the 1.55-μm Telecom Region

For common growth conditions in CBE or MOVPE, InAs/InP (100) QDs always emit at wavelengths far beyond 1.65 μm at room temperature, especially when embedded in quaternary

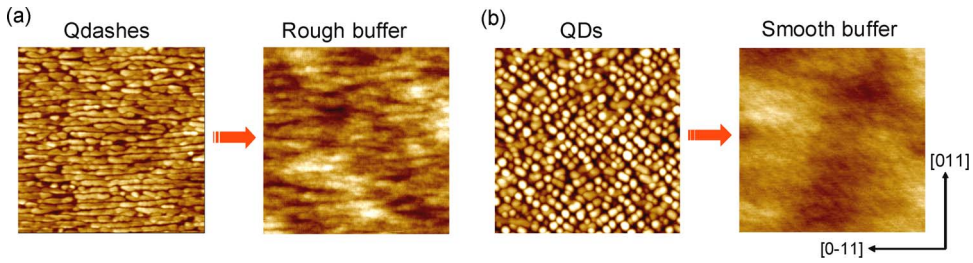

Fig. 1. (a) AFM images of the InAs Qdashes on rough InGaAsP buffer and (b) the InAs QDs on smooth InGaAsP buffer on InP (100). The AFM scan fields are $1 \times 1\ \mu m^2$, and the height contrast is 10 nm for the InAs Qdashes and QDs and 5 nm for the buffer layers. Growth is by CBE.

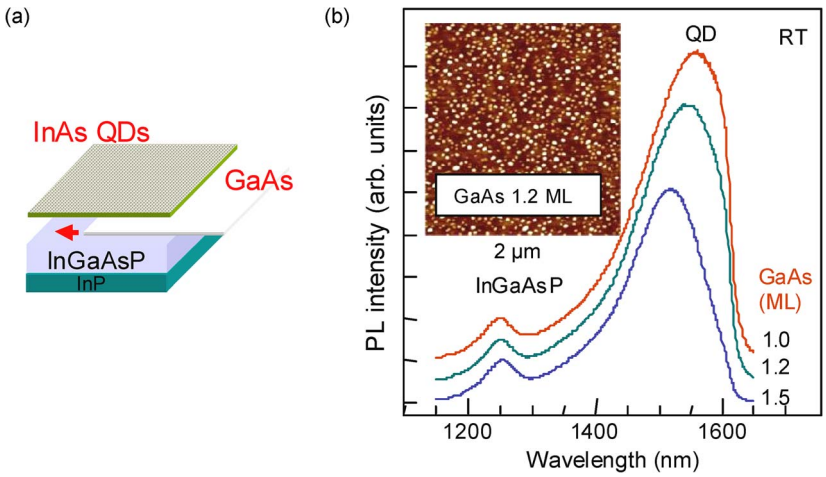

Fig. 2. (a) Scheme of the InAs QDs with GaAs interlayer on InGaAsP/InP (100). (b) PL spectra at room temperature (RT) of the InAs/InGaAsP/InP (100) QDs for varying GaAs interlayer thickness. The inset shows the AFM image of the QDs for a GaAs interlayer thickness of 1.2 ML. The AFM scan field is $2 \times 2\ \mu m^2$, and the height contrast is 10 nm. Growth is by MOVPE.

InGaAsP layers used as waveguide core material in photonic devices. This is due to unavoidable As/P exchange during InAs growth leading to excess formation of InAs rendering the QDs too large. We have solved this problem through the insertion of ultrathin, 1–2 monolayers (ML), GaAs interlayers underneath the QDs [see Fig. 2(a)], first in CBE [7] and later in MOVPE [8] after drastic reduction of growth temperature and group V/III ratio. As a function of thickness, the GaAs interlayers then effectively suppress the unwanted As/P exchange during InAs QD growth to reduce the QD size and, thus, the PL emission wavelength [see Fig. 2(b)]. This, for the first time, allowed the realization of pure InAs/InP (100) QDs with reduced height and small diameter < 15 nm [34] for telecom applications in the 1.55-μm wavelength region at room temperature.

2.2.1. 1.55-μm QD Telecom Devices and QD Mid-Infrared Emission and Devices

Based on these high-quality QDs with emission tuned into the 1.55-μm wavelength region, we have demonstrated

- the first 1.55-μm InAs/InP (100) Fabry–Pérot QD laser operating in continuous-wave (CW) mode at room temperature on the QD ground-state (GS) transition with a stack of five QD layers as gain medium [see Fig. 3(a)] [10];
- the first cleaved-side polarization-insensitive emission at 1.55 μm from close-stacked QDs due to vertical electronic coupling [see Fig. 3(b)], removing the shape anisotropy of the QDs [11];
- polarization control of gain due to interplay of ground and excited QD states [12];
- the first 1.55-μm deeply etched Fabry–Pérot QD laser and QD ring laser not suffering from nonradiative surface recombination [13];

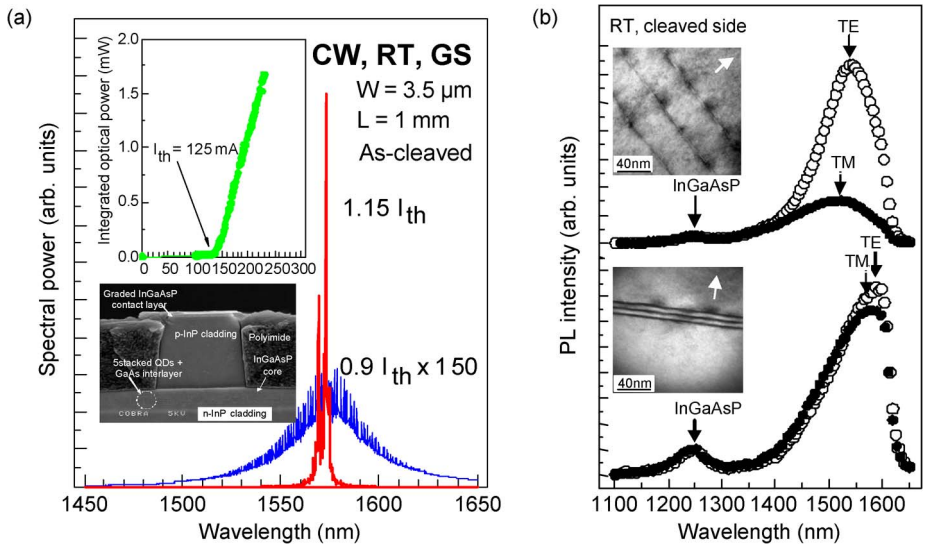

Fig. 3. (a) Amplified spontaneous emission and lasing spectra (CW, room temperature, QD GS) together with the light-current characteristics (upper inset) of the InAs/InGaAsP/InP (100) Fabry–Pérot QD laser shown in the scanning electron microscopy image (lower inset). W and L are the waveguide width and length. (b) Linear polarized PL spectra taken from the cleaved side at room temperature together with cross-sectional transmission electron microscopy images of wide-stacked (upper inset, 40-nm separation layer) and close-stacked (lower inset, 4-nm separation layer) QDs. TE and TM denote transverse electric and transverse magnetic polarization. Growth is by MOVPE.

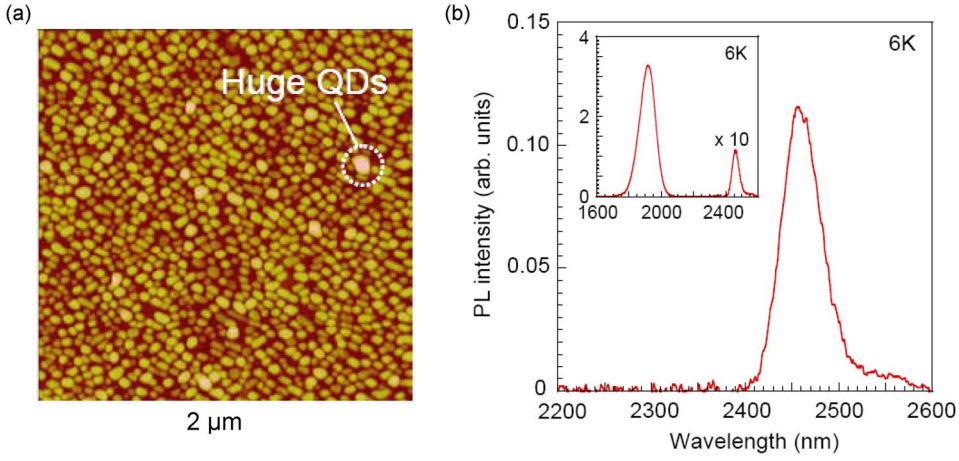

Fig. 4. (a) AFM image of the 1.5-ML InAs QDs on 1.6-nm InAs Qwell structure. The AFM scan field is $2 \times 2\ \mu m^2$, and the height contrast is 40 nm. (b) PL spectrum at 6 K of the huge InAs QDs on QW. Inset: Overview PL spectrum at 6 K showing also the emission of the smaller high-density InAs QDs. Growth is by MOVPE.

- the first 1.55-μm QD microring laser [14];
- the first 1.55-μm QD mode-locked laser [15];
- the first 1.55-μm Butt–joint-integrated extended-cavity QD laser [16];
- the first noninverted 1.55-μm region QD multiwavelength converter [17].

We have also investigated the long-wavelength limit of InAs/InP (100) QDs in the mid-infrared for applications such as medical diagnostics and environmental sensing [35], [36]. After optimizing increased growth temperature and group V/III ratio and exploring various layer structures, including different buffer layers, close QD stacking, and strain-reducing cap layers, we developed a unique InAs QDs on quantum well (Qwell) structure. This QDs on Qwell structure exhibits a high density of

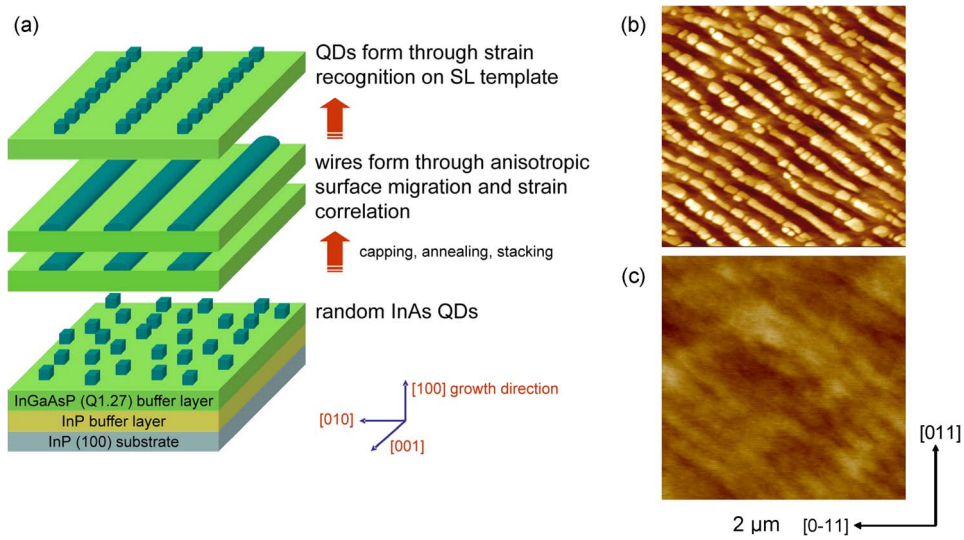

Fig. 5. (a) Scheme of self-organized anisotropic strain engineering for SL template formation and QD ordering on top. (b) AFM images of the linear InAs QD arrays on the optimized SL template, and (c) surface of the SL template. The AFM scan fields in (b) and (c) are $2 \times 2\ \mu m^2$ and the height contrast is (a) 20 nm and (b) 10 nm. Growth is by CBE.

smaller QDs, the density being increased by a factor of 5 to 6 compared with that of the conventional QDs, seen in Fig. 4(a). This made possible the fist demonstration of a single-layer InAs/InP (100) QD laser operating in CW mode at room temperature on the QD GS transition with a lasing wavelength of 1.74 μm [18]. Moreover, the InAs Qwell triggers the formation of sparse huge InAs QDs. These QDs emit at 2.46 μm at low temperature, shown in Fig. 4(b), which is the longest emission wavelength achieved so far in the InAs/InP materials system [9].

3. Linear InAs/InP (100) QD Arrays

3.1. Self-Organized Anisotropic Strain Engineering on InP (100)

Fig. 5(a) shows a scheme of the self-organized InAs/InGaAsP SL template formation for InAs QD ordering by CBE [19]. Starting from a nanoscale random InAs QD layer, subsequent thin InGaAsP capping, anisotropic adatom surface migration during annealing, growth of an InGaAsP separation layer, and strain-correlated repetition in SL growth produces highly ordered 1-D InAs and, thus, strain field modulations on a mesoscopic length scale. InAs QDs on these strain-modulated SL templates arrange into straight, linear single InAs QD arrays due to local strain recognition. Fig. 5(b) shows the InAs QD arrays on the SL template after careful optimization of cap layer thickness and annealing temperature, balancing In desorption and lateral mass transport during annealing, InAs amount, and growth rate, reducing excess strain accumulation and enhancing the In adatom surface migration length and number of SL periods for full development. The optimized growth conditions of the SL template are 505 °C growth temperature, 2.1-ML InAs growth (growth rate 0.23 ML/s), 10-s growth interruption in As flux, 0.3-nm-thin Q1.27 (lattice-matched InGaAsP with room-temperature bandgap at 1.27 μm) capping, 2-min annealing at 520 °C, 15.3-nm Q1.27 separation layer growth, and the number of SL periods of 7. The amount of InAs for QD formation on top of the SL template is 2.6 ML. The alignment of the QD arrays is along [001]. This is along the elastically soft direction of the cubic crystal to minimize the total strain energy. Of the possible [001] and [010] directions, [001] is selected by the substrate miscut 2° toward (110) generating steps in the same direction. This is different to the case of the InAs/GaAs materials system, as studied in [21] and [22], where the linear QD arrays are oriented along [0–11], i.e., along the direction of preferential adatom surface migration related to the surface reconstruction. The SL template surface shown in Fig. 5(c) is very smooth, excluding the formation of multiatomic steps influencing the QD ordering.

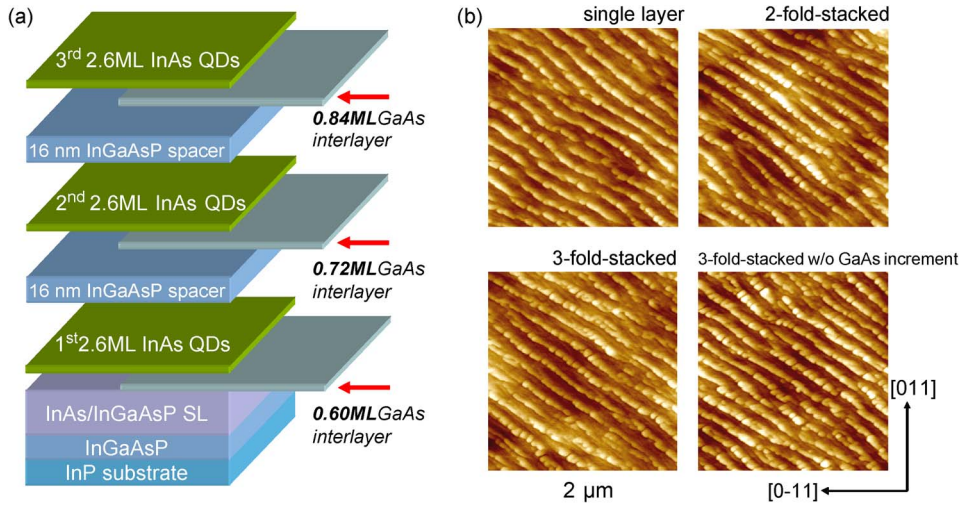

Fig. 6. (a) Scheme of the stacked InAs QD arrays. (b) AFM images of the single-layer, twofold-stacked, and threefold-stacked InAs QD arrays with increment of the GaAs interlayer thickness and of the threefold-stacked arrays without increment. The AFM scan fields in (b) are $2 \times 2\ \mu m^2$, and the height contrast is 10 nm. Growth is by CBE.

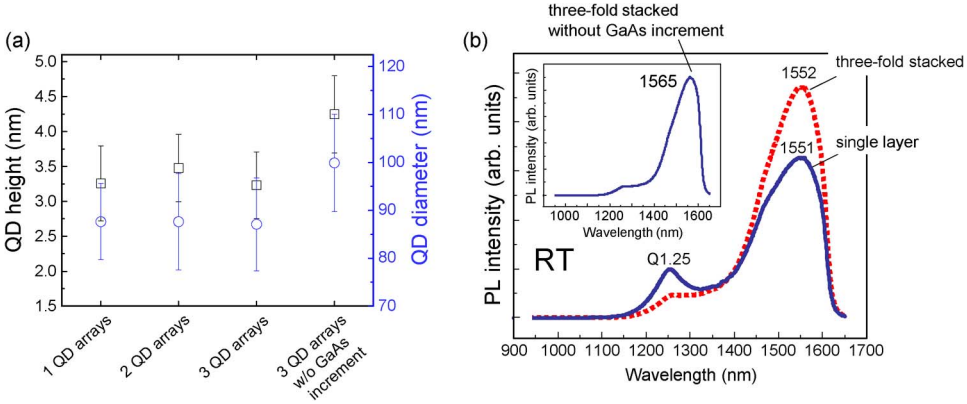

Fig. 7. (a) QD height and diameter of the single layer, twofold-stacked, and threefold-stacked arrays with increment of the GaAs interlayer thickness and of the threefold-stacked arrays without increment. (b) Room-temperature PL spectra of the single-layer and threefold-stacked QD arrays with increment of the GaAs interlayer thickness. Inset: PL spectrum of the threefold-stacked QD arrays without increment.

3.2. Stacked Linear InAs/InP (100) QD Arrays

The linear InAs QD arrays on the optimized SL template are stacked in growth direction with a 16-nm Q1.25 separation layer [20]. Beneath the first layer of QD arrays, a 0.6-ML GaAs interlayer is inserted. In the successively stacked layers of QD arrays, the GaAs interlayer thickness is increased by 0.12 ML, shown schematically in Fig. 6(a). The 0.6-ML GaAs interlayer beneath the first layer of QD arrays reduces the QD height from 7–11 [see Fig. 5(b)] to 3–4 nm [see Fig. 6(b)] without affecting the linear QD ordering. The increment of the GaAs interlayer thickness in successive layers compensates the QD size increase encountered in strain-correlated stacking, which manifests itself in the maintenance of the linear ordering. The QD size is maintained for the twofold- and threefold-stacked QD arrays, shown in Fig. 6(c) and (d). Without increment of the GaAs interlayer thickness, the QD size is clearly increased, shown in Fig. 6(e), for the threefold-stacked QD arrays. The QD height and diameter evolution of the stacked QD arrays with and without increment of the GaAs interlayer thickness is summarized in Fig. 7(a).

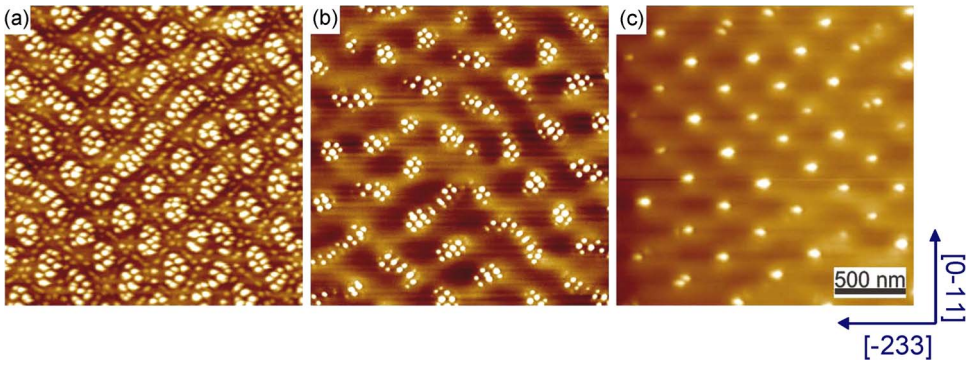

Fig. 8. AFM images of the (a) connected InGaAs QD arrays, (b) isolated InAs QD groups, and (c) single InAs QDs grown on the InGaAs/GaAs SL templates formed by self-organized anisotropic strain engineering on planar GaAs (311)B. The AFM scan fields are $2 \times 2\ \mu m^2$, and the height contrast is 20 nm. Growth is by MBE.

The PL spectra taken at room temperature of the capped (by 100-nm Q1.25 and 50-nm InP) single-layer and threefold-stacked InAs QD arrays with increment of the GaAs interlayer thickness are shown in Fig. 7(b). The insertion of the GaAs interlayers tunes the PL peak wavelength into the 1.55-μm region due to the reduced QD height, and the thickness increment in successive layers guarantees almost identical PL peak wavelength due to the compensation of the QD size increase upon stacking. The PL efficiency of the threefold-stacked QD arrays is increased compared with that of the single-layer QD arrays, indicating good crystal quality of the multilayer-stacked arrays. Without increment of the GaAs interlayer thickness, the PL peak wavelength clearly redshifts due to the increase of the QD size upon stacking, shown in the inset in Fig. 7(b).

The PL efficiency of the QD arrays at room temperature is reduced by about three orders of magnitude compared with that at low temperature due to thermally activated carrier escape from the QDs into the Q barriers, which is confirmed by the activation energy of the PL intensity quenching determined from temperature-dependent PL measurements. Moreover, temperature-dependent measurements of the PL peak energy and linewidth of the QD arrays reveal only a weak indication of "S" shape-like dependence of the PL peak energy and a monotonic increase of the PL linewidth with temperature. Hence, there is only a weak indication of thermally activated carrier redistribution among the QDs through the wetting layer and barriers, as observed for randomly arranged QDs, but a rather strong indication of temperature-independent carrier redistribution due to lateral electronic coupling of the closely spaced QDs within the arrays. This is supported by the linear polarization of the PL along [001], which is the direction of the linear arrays, while the PL of randomly arranged QDs is linearly polarized along [0–11] due to slight elongation in this direction [19].

4. Two-Dimensional and Complex InGaAs/GaAs (311)B QD arrays

4.1. Self-Organized Anisotropic Strain Engineering on GaAs (311)B

Self-organized anisotropic strain engineering of InGaAs/GaAs SL templates on GaAs (311)B by MBE leads to 2-D lateral mesoscopic strain field modulations and the ordering of InGaAs and InAs QDs on top in periodic spot-like arrangements of connected arrays and isolated groups [23]–[25]. The optimized growth conditions of the SL template are 3.3-nm InGaAs (growth rate 0.132 nm/s) grown at 500 °C with In composition of 40%, 10-s growth interruption, thin capping by 0.5-nm GaAs at 500 °C, annealing for 2 min at 600 °C under As_4 flux, growth of a 5.5-nm GaAs separation layer at 600 °C, and number of SL periods of 10. At the top of the SL template, a 3.3-nm InGaAs layer is deposited without annealing for the formation of connected InGaAs QD arrays [see Fig. 8(a)], or 0.6-nm InAs is deposited (growth rate 0.0013 nm/s) at 480 °C after a 15-nm GaAs separation layer

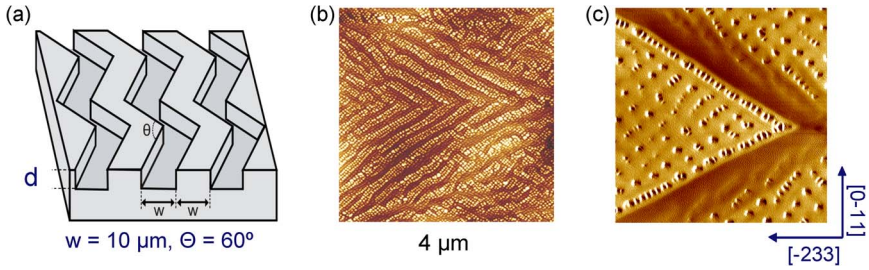

Fig. 9. (a) Scheme of the zigzag mesa structure. (b) Connected InGaAs QD arrays and (c) single InAs QDs on shallow (d = 30 nm), and deep (d = 200 nm) patterned GaAs (311)B. The AFM scan fields in (b) and (c), are 4×4 μm^2, and the height contrast in (b) is 30 nm. In (c), an AFM slope image is shown to reveal the QDs. Growth is by MBE.

for formation of isolated InAs QD groups [see Fig. 8(b)]. Single InAs QDs [see Fig. 8(c)] are formed by increasing the growth temperature of the SL template and InAs layer by about 30 °C while reducing the InAs deposition time to the onset of the reflection high-energy electron diffraction (RHEED) pattern transition from streaky to spotty together with 30-s annealing [26]. Similar QD ordering is observed also in the InAs/InP materials system [37].

4.2. Guided and Directed Self-Organization on Patterned GaAs (311)B

On artificially coarse-patterned GaAs (311)B substrates, guided and directed self-organization is demonstrated to produce complex QD arrays and absolute QD position control. Guided self-organization has also been demonstrated on coarse patterned GaAs (100) substrates [38]. The examined pattern is a periodic zigzag mesa structure shown schematically in Fig. 9(a) fabricated by optical lithography and wet chemical etching. Steps generated on the shallow-patterned (30-nm depth) substrates modify the SL template formation due to change of the direction of adatom surface migration during annealing and, thus, the QD ordering over macroscopic areas, shown in Fig. 9(b) for the connected InGaAs QD arrays. The spot-like arrangement on planar substrates is transformed to a periodic zigzag arrangement of parallel stripes. On deep-patterned (200-nm depth) substrates, the formation of QD-free facets leads to local modification of the QD ordering in rows of dense QDs close to the mesa sidewalls, while the 2-D natural QD ordering on the mesa top and bottom is unaltered. These are two examples of guided self-organization leading to complex QD arrays [25]. Moreover, close inspection of the QD arrays on the deep-patterned substrate reveals that the naturally ordered QD arrays on the mesa top (as well as bottom) are spatially locked to the rows of QDs close to the mesa sidewalls. This results in absolute position control of the QDs over large areas, which is a unique example of directed self-organization [26].

Due to the absence of one-to-one pattern definition, which often degrades the optical quality of ordered QDs [39]–[41], the ordered and position-controlled QDs on the patterned GaAs (311)B substrates exhibit excellent optical quality. This is demonstrated by strong PL emission up to room temperature of the isolated InAs QD groups capped with GaAs on the deep-patterned substrate, shown in Fig. 10(a). Again, the drop in PL efficiency is due to thermal activation of carriers from the InAs QDs into the GaAs barriers. Moreover, individual capped single InAs QDs on the deep-patterned substrate exhibit ultrasharp emission with resolution limited (80 μeV) linewidth at low temperature, which is demonstrated in the micro-PL spectrum shown in Fig. 10(b) [26].

5. InAs QD Distribution and Number Control on Truncated InP (100) Pyramids

5.1. Selective InP (100) Pyramid Growth and Regrowth Scheme

InP pyramids containing InAs QDs are selectively grown by MOVPE in SiN_x mask openings of various sizes and shapes fabricated by electron beam lithography and reactive ion etching on InP (100). The growth conditions are 610 °C growth temperature, 18.39-nm/min growth rate, and a total

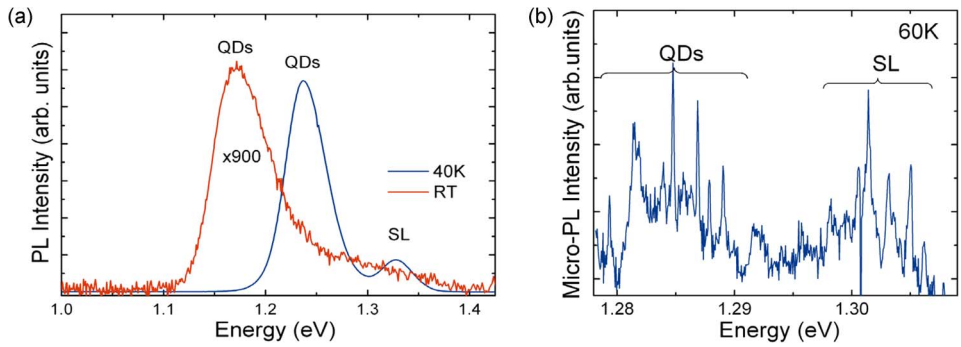

Fig. 10. (a) Low- and room-temperature PL spectra of the isolated InAs QD groups and (b) low-temperature micro-PL spectrum of the single InAs QDs on deep-patterned GaAs (311)B.

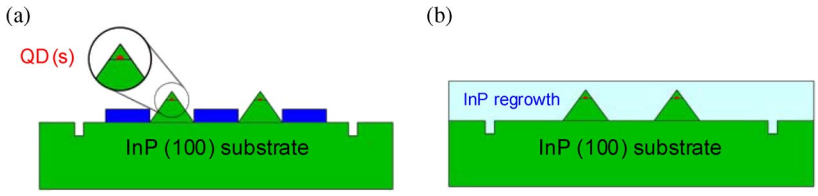

Fig. 11. (a) Scheme of selective-area growth of InP (100) pyramids containing InAs QDs and (b) of InP regrowth around the pyramids.

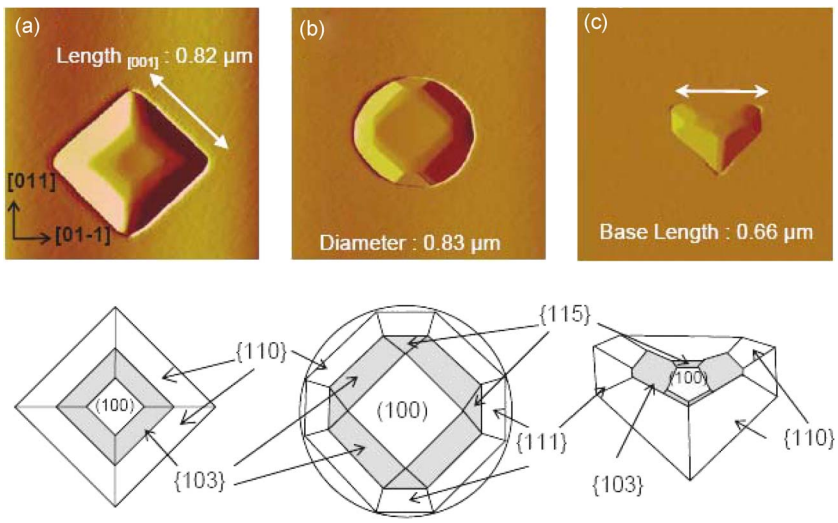

Fig. 12. AFM images of the truncated InP (100) pyramids together with schematic drawings with (a) square, (b) circular, and (c) triangular base. The scan fields are $2 \times 2\ \mu m^2$. Growth is by MOVPE.

thickness of 75 nm in unmasked areas. After removal of the SiN_x mask, passive InP structures are grown at temperatures between 550 and 630 °C around the pyramids for planarization. The scheme of the growth sequence is presented in Fig. 11(a) and (b). In Fig. 12, the truncated InP pyramids with (a) square, (b) circular, and (c) triangular mask openings, i.e., pyramid bases are shown, together with schematic drawings. The pyramid sidewalls are bound by {110} and {111} facets. The pyramid top surfaces are composed of a (100) central facet and high-index {103} and {115} facets around. The facet composition of the pyramid top surfaces, i.e., the facet types, shapes, arrangements, and their (relative) sizes, are distinctly determined by the shapes of the pyramid bases and the sizes of the top surface areas [27].

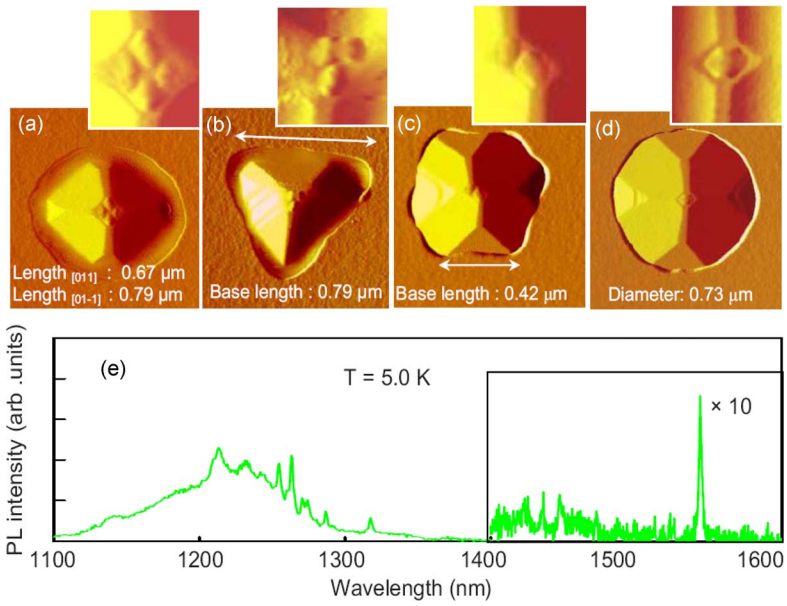

Fig. 13. (a)–(d) Elliptical, triangular, hexagonal, and circular-based InP pyramids close to pinch-off, together with magnified images of the four, three, two, and single InAs QDs on top. (e) Micro-PL spectrum from a single capped InAs QD on a circular-based InP pyramid. The scan fields are 1×1 μm^2 and 0.2×0.2 μm^2. Growth is by MOVPE.

5.2. InAs QD Positioning and Regrowth

The control of the facet composition of the pyramid top surfaces by the shapes of the pyramid bases and sizes of the top surface areas allows the distribution and number control of the InAs QDs grown on top [27]. QD positioning on patterned substrates and selectively grown structures has been widely studied [42]–[50] but not the detailed impact of the shape. The QDs, which are grown at 515 °C with 3-ML InAs supply, preferentially nucleate on the high-index facets on the pyramid top surfaces, hence, assuming their arrangement while the QD number is directly related to the (relative) sizes of the facets. Ultimately, this allows matching of the QD distribution to the photon mode of an optical cavity, e.g., photonic crystal defect, microdisk, or ring, to guarantee maximum coupling accompanied with lowest possible losses. Below a certain size of the pyramid top surface areas, only the (100) central facets remain, and the QDs uniformly nucleate thereon. Close to pinch-off, four, three, two, and single QDs are positioned around/at the center, with the QD number being related to the pyramid base shapes. Four for elliptical base, three for triangular base, two for hexagonal base, and a single QD for circular base, as shown in Fig. 13(a)–(d). It is, hence, the combination of the pyramid top (100) facet shapes and their sizes that determines the QD number. High optical quality of the QDs is guaranteed by the sufficient separation of the processed surface and the QDs and is revealed by the micro-PL spectrum of a single InP capped QD on a circular-based pyramid at 5 K, shown in Fig. 13(e). The broad emission around 1200–1300 nm is attributed to the InAs wetting layer on the pyramid side facets. The single sharp peak at 1542 nm with resolution-limited linewidth of 2 nm stems from the single position-controlled InAs QD. Again, the PL is tuned into the 1.55-μm telecom wavelength region through the insertion of an ultrathin GaAs interlayer.

To explore submicrometer active–passive integration, which was previously introduced for larger InP pyramids grown in SiN_x mask openings fabricated by optical lithography [51], regrowth of a passive InP structure is performed after removal of the SiN_x mask [52]. Taking advantage of the lateral growth behavior of InP, this results, independent of the shapes of the pyramids, in smooth, uniform, planar layers around the pyramids at elevated growth temperature. Fig. 14 shows the morphology of the regrown InP structures for different growth temperatures.

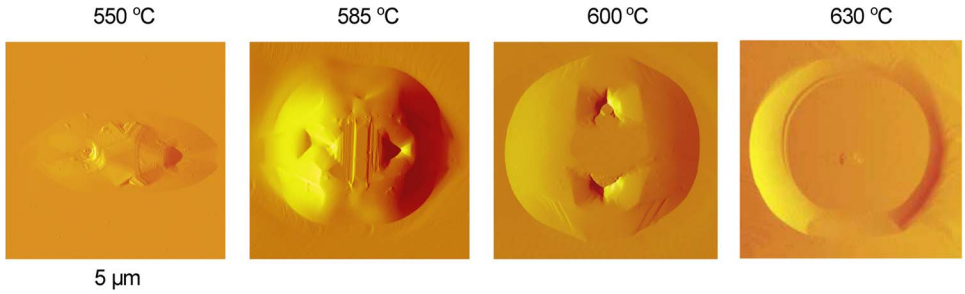

Fig. 14. AFM images of the regrown passive InP structures around the InP pyramids containing InP capped InAs QDs for different growth temperatures. The AFM scan fields are 5×5 μm^2. Growth is by MOVPE.

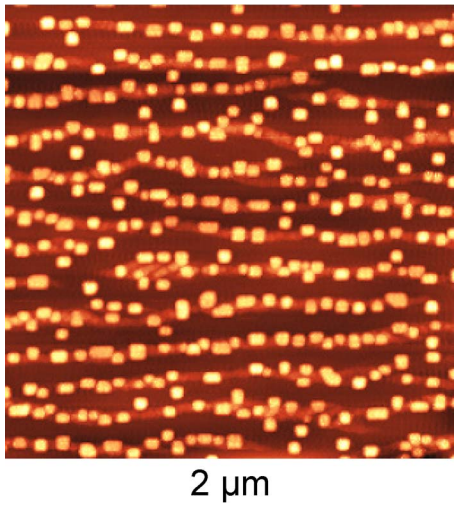

Fig. 15. AFM image of In nanocrystals aligned on linear InGaAs QD arrays on an InGaAs/GaAs SL template formed by self-organized anisotropic strain engineering on GaAs (100). The AFM scan field is 2×2 μm^2. Growth is by MBE.

6. Conclusion

First, general aspects of InAs/InP (100) QDs regarding formation of QDs versus Qdashes, wavelength tuning from telecom to mid-infrared region, and device applications have been discussed. Then, our recent progress on the lateral ordering, position, and number control of QDs have been described, based on self-organized anisotropic strain engineering, growth on patterned substrates, and selective-area growth. Single-layer and stacked linear InAs QD arrays were formed by self-organized anisotropic strain engineering of an InAs/InGaAsP SL template on InP (100) with emission wavelength at room temperature in the important 1.55-μm telecom wavelength region. Guided and directed self-organized anisotropic strain engineering was demonstrated on shallow- and deep-patterned GaAs (311)B for formation of complex InAs QD arrays and absolute QD position control. Lateral position, distribution, and number control of InAs QDs, down to a single QD, was demonstrated on truncated InP (100) pyramids by selective-area growth with sharp emission at 1.55 μm. Submicrometer-scale active–passive integration was established by lateral regrowth of InP around the pyramids for planarization. The demonstrated control over QD formation is the key to future quantum functional nanophotonic devices and integrated circuits operating at the single and multiple electron and photon level with controlled quantum mechanical and electromagnetic interactions.

We made a significant step forward in applying our concept of self-organized anisotropic strain engineering to the alignment of metal nanocrystals and metal nanocrystal arrays on top of ordered InGaAs QD arrays (see Fig. 15). This made possible hybrid semiconductor QD–metal nanocrystal nanostructures and arrays with nanometer-scale precise lateral and vertical site registration, thus opening the door to the exciting field of coupled Plasmon–QD physics and applications. Coupled Plasmon–QD emission has already been observed [53].

Acknowledgment

The author thanks N. Sritirawisarn, E. Selcuk, H. Wang, J. Yuan, J. Kotani, and S. Anantathanasarn for the very fruitful collaboration.

References

[1] R. Nötzel, T. Mano, Q. Gong, and J. H. Wolter, "Self-organized anisotropic strain engineering: A new concept for quantum dot ordering," *Proc. IEEE*, vol. 91, no. 11, pp. 1898–1906, Nov. 2003 (Invited Paper).
[2] R. Nötzel, N. Sritirawisarn, E. Selçuk, and S. Anantathanasarn, "Lateral ordering, position, and number control of self-organized quantum dots: The key to future functional nanophotonic devices," *IEEE J. Sel. Topics Quantum Electron.*, vol. 14, no. 4, pp. 1140–1149, Jul./Aug. 2008 (Invited Paper).
[3] M. Ohtsu, T. Kawazoe, T. Yatsui, and M. Naruse, "Nanophotonics: Application of dressed photons to novel photonic devices and systems," *IEEE J. Sel. Topics Quantum Electron.*, vol. 14, no. 6, pp. 1404–1417, Nov./Dec. 2008.
[4] R. J. Young, D. J. P. Ellis, R. M. Stevenson, A. J. Bennett, P. Atkinson, K. Cooper, D. A. Ritchie, and A. J. Shields, "Quantum-dot sources for single photons and entangled photon pairs," *Proc. IEEE*, vol. 95, no. 9, pp. 1805–1814, Sep. 2007.
[5] R. Hafenbrak, S. M. Ulrich, P. Michler, L. Wang, A. Rastelli, and O. G. Schmidt, "Triggered polarization-entangled photon pairs from a single quantum dot up to 30 K," *New J. Phys.*, vol. 9, no. 9, p. 315, Sep. 2007.
[6] N. Sritirawisarn, F. W. M. van Otten, T. J. Eijkemans, and R. Nötzel, "Surface morphology induced InAs quantum dot or dash formation on InGaAsP/InP (100)," *J. Cryst. Growth*, vol. 305, no. 1, pp. 63–69, Jul. 2007.
[7] Q. Gong, R. Nötzel, P. J. van Veldhoven, T. J. Eijkemans, and J. H. Wolter, "Wavelength tuning of InAs quantum dots grown on InP (100) by chemical-beam epitaxy," *Appl. Phys. Lett.*, vol. 84, no. 2, pp. 275–277, Jan. 2004.
[8] S. Anantathanasarn, R. Nötzel, P. J. van Veldhoven, T. J. Eijkemans, and J. H. Wolter, "Wavelength-tunable (1.55-μm region) InAs quantum dots in InGaAsP/InP (100) grown by metal–organic vapor phase epitaxy," *J. Appl. Phys.*, vol. 98, no. 1, pp. 013503-1–013503-7, Jul. 2005.
[9] J. Kotani, P. J. van Veldhoven, and R. Nötzel, "Mid-infrared emission from InAs quantum dots, wells, and dots on well nanostructures grown on InP (100) by metal organic vapor phase epitaxy," *J. Appl. Phys.*, vol. 106, no. 9, pp. 093112-1–093112-5, Nov. 2009.
[10] S. Anantathanasarn, R. Nötzel, P. J. van Veldhoven, F. W. M. van Otten, Y. Barbarin, G. Servanton, T. de Vries, E. Smalbrugge, E. J. Geluk, T. J. Eijkemans, E. A. J. M. Bente, Y. S. Oei, M. K. Smit, and J. H. Wolter, "Lasing of wavelength-tunable (1.55 μm region) InAs/InGaAsP/InP (100) quantum dots grown by metal organic vapor-phase epitaxy," *Appl. Phys. Lett.*, vol. 89, no. 7, pp. 073115-1–073115-3, Aug. 2006.
[11] S. Anantathanasarn, R. Nötzel, P. J. van Veldhoven, F. W. M. van Otten, T. J. Eijkemans, and J. H. Wolter, "Stacking and polarization control of wavelength-tunable (1.55 μm region) InAs/InGaAsP/InP (100) quantum dots," *Appl. Phys. Lett.*, vol. 88, no. 6, pp. 063105-1–063105-3, Feb. 2006.
[12] S. Anantathanasarn, P. J. van Veldhoven, T. J. Eijkemans, T. de Vries, E. Smalbrugge, E. J. Geluk, E. A. J. M. Bente, Y. S. Oei, M. K. Smit, and R. Nötzel, "Polarization control of gain of stacked InAs/InP (100) quantum dots at 1.55 μm: Interplay between ground and excited state transitions," *Appl. Phys. Lett.*, vol. 92, no. 12, pp. 123113-1–123113-3, Mar. 2008.
[13] Y. Barbarin, S. Anantathanasarn, E. A. J. M. Bente, Y. S. Oei, M. K. Smit, and R. Nötzel, "1.55-μm range InAs-InP (100) quantum-dot Fabry–Perot and ring lasers using narrow deeply etched ridge waveguides," *IEEE Photon. Technol. Lett.*, vol. 18, no. 24, pp. 2644–2646, Dec. 2006.
[14] M. T. Hill, S. Anantathanasarn, Y. Zhu, Y. S. Oei, P. J. van Veldhoven, M. K. Smit, and R. Nötzel, "InAs-InP (1.55-μm region) quantum-dot microring lasers," *IEEE Photon. Technol. Lett.*, vol. 20, no. 6, pp. 446–448, Mar. 2008.
[15] M. J. R. Heck, E. A. J. M. Bente, E. Smalbrugge, Y. S. Oei, M. K. Smit, S. Anantathanasarn, and R. Nötzel, "Observation of Q-switching and mode-locking in two-section InAs/InP (100) quantum dot lasers around 1.55 μm," *Opt. Express*, vol. 15, no. 25, pp. 16 292–16 301, Dec. 2007.
[16] H. Wang, J. Yuan, P. J. van Veldhoven, T. de Vries, B. Smalbrugge, E. J. Geluk, E. A. J. M. Bente, Y. S. Oei, M. K. Smit, S. Anantathanasarn, and R. Nötzel, "Butt joint integrated extended cavity InAs/InP (100) quantum dot laser emitting around 1.55 μm," *Electron. Lett.*, vol. 44, no. 8, pp. 522–523, Apr. 2008.
[17] O. Raz, J. Herrera, N. Calabretta, E. Tangdiongga, S. Anantathanasarn, R. Nötzel, and H. J. S. Dorren, "Non-inverted multiple wavelength converter at 40 Gbit/s using 1550 nm quantum dot SOA," *Electron. Lett.*, vol. 44, no. 16, pp. 988–989, Jul. 2008.
[18] J. Kotani, P. J. van Veldhoven, T. de Vries, B. Smalbrugge, E. A. J. M. Bente, M. K. Smit, and R. Nötzel, "First demonstration of single-layer InAs/InP (100) quantum-dot laser: Continuous wave, room temperature, ground state," *Electron. Lett.*, vol. 45, no. 25, pp. 1317–1318, Dec. 2009.

[19] N. Sritirawisarn, F. W. M. van Otten, T. J. Eijkemans, and R. Nötzel, "Formation of linear InAs quantum dot arrays on InGaAsP/InP (100) by self-organized anisotropic strain engineering and their optical properties," *J. Appl. Phys.*, vol. 102, no. 5, pp. 053514-1–053514-7, Sep. 2007.
[20] N. Sritirawisarn, F. W. M. van Otten, T. J. Eijkemans, and R. Nötzel, "Wavelength controlled multilayer-stacked linear InAs quantum dot arrays on InGaAsP/InP (100) by self-organized anisotropic strain engineering: A self-ordered quantum dot crystal," *Appl. Phys. Lett.*, vol. 93, no. 13, pp. 131 906-1–131 906-3, Sep. 2008.
[21] T. Mano, R. Nötzel, G. J. Hamhuis, T. J. Eijkemans, and J. H. Wolter, "Formation of InAs quantum dot arrays on GaAs (100) by self-organized anisotropic strain engineering of a (In,Ga)As superlattice template," *Appl. Phys. Lett.*, vol. 81, no. 9, pp. 1705–1707, Aug. 2002.
[22] T. Mano, R. Nötzel, G. J. Hamhuis, T. J. Eijkemans, and J. H. Wolter, "Direct imaging of self-organized anisotropic strain engineering for improved one-dimensional ordering of (In,Ga)As quantum dot arrays," *J. Appl. Phys.*, vol. 95, no. 1, pp. 109–114, Jan. 2004.
[23] T. van Lippen, R. Nötzel, G. J. Hamhuis, and J. H. Wolter, "Self-organized lattice of ordered quantum dot molecules," *Appl. Phys. Lett.*, vol. 85, no. 1, pp. 118–120, Jul. 2004.
[24] T. van. Lippen, R. Nötzel, G. J. Hamhuis, and J. H. Wolter, "Ordered quantum dot molecules and single quantum dots by self-organized anisotropic strain engineering," *J. Appl. Phys.*, vol. 97, no. 4, pp. 044 301-1–044 301-6, Feb. 2005.
[25] E. Selcuk, G. J. Hamhuis, and R. Nötzel, "Complex laterally ordered InGaAs and InAs quantum dots by guided self-organized anisotropic strain engineering on shallow- and deep-patterned GaAs (311)B substrates," *J. Appl. Phys.*, vol. 102, no. 9, pp. 094 301-1–094 301-5, Nov. 2007.
[26] E. Selcuk, A. Y. Silov, and R. Nötzel, "Single InAs quantum dot arrays and directed self-organization on patterned GaAs (311)B substrates," *Appl. Phys. Lett.*, vol. 94, no. 26, pp. 263 108-1–263 108-3, Jun. 2009.
[27] H. Wang, J. Yuan, T. Rieger, P. J. van Veldhoven, P. Nouwens, T. J. Eijkemans, T. de Vries, B. Smalbrugge, E. J. Geluk, and R. Nötzel, "Distribution control of 1.55μm InAs quantum dots down to small numbers on truncated InP pyramids grown by selective area metal organic vapor phase epitaxy," *Appl. Phys. Lett.*, vol. 94, no. 14, pp. 143103-1–143103-3, Apr. 2009.
[28] J. Brault, M. Gendry, G. Grenet, G. Hollinger, Y. Desieres, and T. Benyattou, "Role of buffer surface morphology and alloying effects on the properties of InAs nanostructures grown on InP(001)," *Appl. Phys. Lett.*, vol. 73, no. 20, pp. 2932–2934, Nov. 1998.
[29] L. Gonzalez, J. M. Garcia, R. Garcia, F. Briones, J. Martinez-Pastor, and C. Ballesteros, "Influence of buffer-layer surface morphology on the self-organized growth of InAs on InP(001) nanostructures," *Appl. Phys. Lett.*, vol. 76, no. 9, pp. 1104–1106, Feb. 2000.
[30] C. Walther, W. Hoerstel, H. Niehus, J. Erxmeyer, and W. T. Masselink, "Growth, structural, and electrical investigation of self-assembled InAs quantum wires on (001)InP," *J. Cryst. Growth*, vol. 209, no. 4, pp. 572–580, Feb. 2000.
[31] Z. H. Zhang, G. W. Pickrell, K. L. Chang, H. C. Lin, K. C. Hsieh, and K. Y. Cheng, "Surface morphology control of InAs nanostructures grown on InGaAs/InP," *Appl. Phys. Lett.*, vol. 82, no. 25, pp. 4555–4557, Jun. 2003.
[32] A. Stintz, T. J. Rotter, and K. J. Malloy, "Formation of quantum wires and quantum dots on buffer layers grown on InP substrates," *J. Cryst. Growth*, vol. 255, no. 3/4, pp. 266–272, Aug. 2003.
[33] H. J. Parry, M. J. Ashwin, and T. S. Jones, "InAs nanowire formation on InP(001)," *J. Appl. Phys.*, vol. 100, no. 11, pp. 114305-1–114305-7, Dec. 2006.
[34] J. M. Ulloa, S. Anantathanasarn, P. J. van Veldhoven, P. M. Koenraad, and R. Notzel, "Influence of an ultrathin GaAs interlayer on the structural properties of InAs/InGaAsP/InP (001) quantum dot's investigated by cross-sectional scanning tunneling microscopy," *Appl. Phys. Lett.*, vol. 92, no. 8, pp. 083 103-1–083 103-3, Feb. 2008.
[35] U. Sharma, E. W. Chang, and S. H. Yun, "Long-wavelength optical coherence tomography at 1.7 μm for enhanced imaging depth," *Opt. Express*, vol. 16, no. 24, pp. 19 712–19 723, Nov. 2008.
[36] W. Lei and C. Jagadish, "Lasers and photodetectors for mid-infrared 2-3 μm applications," *J. Appl. Phys.*, vol. 104, no. 9, pp. 091101-1–091101-11, Nov. 2008.
[37] N. Sritirawisarn, F. W. M. van Otten, P. E. D. Soto Rodriguez, J. L. E. Wera, and R. Nötzel, "Formation of two-dimensional InAs quantum dot arrays by self-organized anisotropic strain engineering on InP (311)B substrates," *J. Cryst. Growth*, vol. 312, no. 2, pp. 164–168, Jan. 2010.
[38] T. Mano, R. Nötzel, D. Zhou, G. J. Hamhuis, T. J. Eijkemans, and J. H. Wolter, "Complex quantum dot arrays formed by combination of self-organized anisotropic strain engineering and step engineering on shallow patterned substrates," *J. Appl. Phys.*, vol. 97, no. 1, pp. 014304-1–014304-5, Jan. 2005.
[39] S. Kiravittaya, A. Rastelli, and O. G. Schmidt, "Self-assembled InAs quantum dots on patterned GaAs(001) substrates: Formation and shape evolution," *Appl. Phys. Lett.*, vol. 87, no. 24, pp. 243112-1–243112-3, Dec. 2005.
[40] S. Ohkouchi, Y. Nakamura, H. Nakamura, and K. Asakawa, "InAs nano-dot array formation using nano-jet probe for photonics applications," *Jpn. J. Appl. Phys.*, vol. 44, no. 7B, pp. 5777–5789, Jul. 2005.
[41] P. Atkinson, S. P. Bremner, D. Anderson, G. A. C. Jones, and D. A. Ritchie, "Size evolution of site-controlled InAs quantum dots grown by molecular beam epitaxy on prepatterned GaAs substrates," *J. Vac. Sci. Technol. B, Microelectron. Process. Phenom.*, vol. 24, no. 3, pp. 1523–1526, May 2006.
[42] W. Seifert, N. Carlsson, A. Petersson, L.-E. Wernersson, and L. Samuelson, "Alignment of InP Stranski–Krastanow dots by growth on patterned GaAs/GaInP surfaces," *Appl. Phys. Lett.*, vol. 68, no. 12, pp. 1684–1686, Mar. 1996.
[43] R. Zhang, R. Tsui, K. Shiralagi, and H. Goronkin, "Spatially selective formation of InAs self-organized quantum dots on patterned GaAs (100) substrates," *Jpn. J. Appl. Phys.*, vol. 38, no. 1B, pp. 455–458, Jan. 1999.
[44] H. Lee, J. A. Johnson, M. Y. He, J. S. Speck, and P. M. Petroff, "Strain-engineered self-assembled semiconductor quantum dot lattices," *Appl. Phys. Lett.*, vol. 78, no. 1, pp. 105–107, Jan. 2001.
[45] C.-K. Hahn, J. Motohisa, and T. Fukui, "Formation of single and double self-organized InAs quantum dot by selective area metal-organic vapor phase epitaxy," *Appl. Phys. Lett.*, vol. 76, no. 28, pp. 3947–3949, Jun. 2000.
[46] J. Tatebayashi, M. Nishioka, T. Someya, and Y. Arakawa, "Area-controlled growth of InAs quantum dots and improvement of density and size distribution," *Appl. Phys. Lett.*, vol. 77, no. 21, pp. 3382–3384, Nov. 2000.

[47] P. S. Wong, G. Balakrishnan, N. Nuntawong, J. Tatebayashi, and D. L. Huffaker, "Controlled InAs quantum dot nucleation on faceted nanopatterned pyramids," *Appl. Phys. Lett.*, vol. 90, no. 18, pp. 183 103-1–183 103-3, Apr. 2007.
[48] D. Chithrani, R. L. Williams, J. Lefebvre, P. J. Poole, and G. C. Aers, "Optical spectroscopy of single, site-selected, InAs/InP self-assembled quantum dots," *Appl. Phys. Lett.*, vol. 84, no. 6, pp. 978–980, Feb. 2004.
[49] T.-P. Hsieh, J.-I. Chyi, H.-S. Chang, W.-Y. Chen, T. M. Hsu, and W. H. Chang, "Single photon emission from an InGaAs quantum dot precisely positioned on a nano-plane," *Appl. Phys. Lett.*, vol. 90, no. 7, pp. 073 105-1–073 105-3, Feb. 2007.
[50] T. Tran, A. Muller, C. K. Shih, P. S. Wong, G. Balakrishnan, N. Nuntawong, J. Tatebayashi, and D. L. Huffaker, "Single dot spectroscopy of site-controlled InAs quantum dots nucleated on GaAs nanopyramids," *Appl. Phys. Lett.*, vol. 91, no. 13, pp. 133104-1–133104-3, Sep. 2007.
[51] D. Zhou, S. Anantathanasarn, P. J. van Veldhoven, F. W. M. van Otten, T. J. Eijkemans, T. de Vries, E. Smalbrugge, and R. Nötzel, "Submicron active-passive integration with position and number controlled InAs/InP (100) quantum dots (1.55 μm wavelength region) by selective-area growth," *Appl. Phys. Lett.*, vol. 91, no. 13, pp. 131102-1–131102-3, Sep. 2007.
[52] J. Yuan, H. Wang, P. J. van Veldhoven, T. Rieger, P. Nouwens, T. J. Eijkemans, T. de Vries, B. Smalbrugge, E. J. Geluk, and R. Nötzel, "1.55 μm InAs quantum dot distribution on truncated InP pyramids and regrowth by selective area epitaxy," in *Proc. IOP Conf. Ser., Mater. Sci. Eng.*, Nov. 2009, vol. 6, pp. 012004-1–012004-4.
[53] A. Urbanczyk, G. J. Hamhuis, and R. Nötzel, *Appl. Phys. Lett.*, submitted for publication.